Journal of Power Sources 195 (2010) 6516–6523

Contents lists available at ScienceDirect

Journal of Power Sources

journal homepage: www.elsevier.com/locate/jpowsour

Raney-platinum film electrodes for potentially implantable glucose fuel cells. Part 1: Nickel-free glucose oxidation anodes

S. Kerzenmacher[a,*], M. Schroeder[b], R. Brämer[c], R. Zengerle[a,d], F. von Stetten[a]

[a] Laboratory for MEMS Applications, Department of Microsystems Engineering- IMTEK, University of Freiburg, Georges-Koehler-Allee 106, 79110 Freiburg, Germany
[b] Institut für Anorganische und Analytische Chemie, University of Freiburg, Albertstrasse 21, 79104 Freiburg, Germany
[c] Hochschule Offenburg- University of Applied Sciences, Badstrasse 24, 79652 Offenburg, Germany
[d] Centre for Biological Signalling Studies (bioss), Albert-Ludwigs-Universität Freiburg, Germany

ARTICLE INFO

Article history:
Received 22 January 2010
Received in revised form 9 April 2010
Accepted 13 April 2010
Available online 18 April 2010

Keywords:
Glucose fuel cell
Implantable
Raney
Platinum
Zinc
Artificial tissue fluid

ABSTRACT

We present a novel fabrication route yielding Raney-platinum film electrodes intended as glucose oxidation anodes for potentially implantable fuel cells. Fabrication roots on thermal alloying of an extractable metal with bulk platinum at 200 °C for 48 h. In contrast to earlier works using carcinogenic nickel, we employ zinc as potentially biocompatible alloying partner. Microstructure analysis indicates that after removal of extractable zinc the porous Raney-platinum film (roughness factor ~2700) consists predominantly of the Pt_3Zn phase. Release of zinc during electrode operation can be expected to have no significant effect on physiological normal levels in blood and serum, which promises good biocompatibility. In contrast to previous anodes based on hydrogel-bound catalyst particles the novel anodes exhibit excellent resistance against hydrolytic and oxidative attack. Furthermore, they exhibit significantly lower polarization with up to approximately 100 mV more negative electrode potentials in the current density range relevant for fuel cell operation. The anodes' amenability to surface modification with protective polymers is demonstrated by the exemplary application of an approximately 300 nm thin Nafion coating. This had only a marginal effect on the anode long-term stability and amino acid tolerance. While in physiological glucose solution after approximately 100 h of operation gradually increasing performance degradation occurs, rapid electrode polarization within 24 h is observed in artificial tissue fluid. Optimization approaches may include catalyst enhancement by adatom surface modification and the application of specifically designed protective polymers with controlled charge and mesh size.

1. Introduction

Implantable glucose fuel cells employing abiotic catalysts (e.g. noble metals, activated carbon) are currently under consideration to realize a battery-independent power supply for medical implants [1,2]. These fuel cells directly generate electrical energy from the electrochemical reaction of glucose and oxygen available in body fluids. In previous prototypes both, cathode and anode have been fabricated mainly from hydrogel-embedded catalyst particles [2–8]. However, the application of hydrogel-polymers as structural component results in a complex system. On the one hand the hydrogel has to be mechanically and chemically stable to maintain structural integrity of the electrode. Here in particular poly(vinyl alcohol)–poly(acrylic acid) hydrogels used in previous works are susceptible to hydrolytic and oxidative attack upon prolonged electrode operation [8]. On the other hand the hydrogel must be sufficiently permeable to allow for the reactants to reach the catalyst surface. Furthermore, the presence of a hydrogel matrix for structural support of the catalyst particles renders the additional application of specific polymers to favorably influence catalytic behavior [9,10] and to reduce electrode poisoning [10–12] difficult.

An attractive alternative electrode fabrication concept that obviates the need for hydrogel binders has been reported by Gebhardt et al. [13]. They fabricated Raney-platinum film anodes by extraction of the non-noble component from annealed platinum–nickel bi-layers or homogenous alloy foils fabricated from a fusible regulus. Compared to conventional anodes, these anodes exhibited improved glucose oxidation performance as well as excellent resistance against oxidative and hydrolytic attack. However, the use of nickel as non-noble, extractable component is likely to be problematic in the context of implantable electrodes due to its allergenic and carcinogenic properties [14]. Nickel cannot be completely extracted from the alloy [13], and thus trace amounts might leach upon operation of the electrode and provoke immunogenic reactions of the body tissue. To solve this problem, a more suitable, biocompatible alloying partner would be required. A promising alternative can-

* Corresponding author. Tel.: +49 761 2037328; fax: +49 761 2037322.
E-mail address: kerzenma@imtek.de (S. Kerzenmacher).

0378-7753/$ – see front matter © 2010 Elsevier B.V. All rights reserved.
doi:10.1016/j.jpowsour.2010.04.039

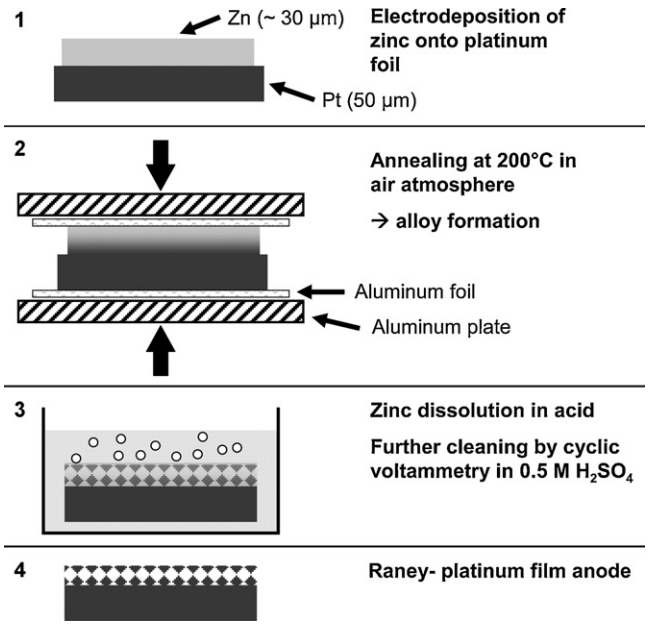

Fig. 1. Schematic of the anode fabrication processes. See text for explanations.

didate forming alloys with platinum [15] is zinc, which in terms of potential biocompatibility can be regarded as less problematic compared to nickel. Zinc's considerable mean concentration in the human body is as high as 6.5 mg l^{-1} in blood and 1 mg l^{-1}in serum [16], which renders the possible leaching of trace amounts from electrodes insignificant.

The aim of the present work is to develop a nickel-free fabrication route for Raney-platinum film anodes using zinc as alloying partner, and evaluate their applicability as anodes in potentially implantable glucose fuel cells. Thereto their current density–potential behavior upon glucose electro-oxidation is investigated under physiologically relevant conditions, including the presence of endogenous amino acids in artificial tissue fluid. Special care is given to obtain significant performance data by carrying out triplicate experiments and by recording polarization curves with a stepwise galvanostatic technique (multi-step chronopotentiometry), which prevents performance overestimation resulting from too fast current sweep rates [17].

Furthermore included into the study is the characterization of the electrode material by means of X-ray diffraction (XRD) and energy-dispersive X-ray spectroscopy (EDX), the analysis of metal-leaching upon prolonged electrode operation, and the exemplary application of a thin Nafion layer as easy to implement polymer modification. Considered to be biocompatible [18,19], Nafion has successfully been applied in the field of biosensors to reject anionic interferents such as ascorbic and uric acid [20] and acetaminophen (paracetamol) [19], and to improve the response of non-enzymatic glucose sensors in human plasma [21].

The fabrication of Raney-platinum film electrodes for cathodic oxygen reduction using aluminum as alloying partner will be reported in part two of this paper series [22].

2. Experimental

2.1. Fabrication of Raney-platinum anodes

The general fabrication process is shown schematically in Fig. 1 and described in the following. As substrates 17 mm × 17 mm pieces of 50 µm platinum foil (Chempur GmbH, Karlsruhe/Germany) were mounted together with two platinum wires for electrical connection between silicone rubber gaskets in the polycarbonate frame described elsewhere [17], exposing only a 15 mm × 15 mm section of one side of the foil. The exposed surface was cleaned by 10 cyclic voltammetry sweeps at 10 mV s^{-1} between 1.3 and −0.3 V vs. a saturated calomel reference electrode (SCE) in de-aerated (nitrogen-purged) 0.5 M H_2SO_4 (Merck KGaA, Darmstadt/Germany).

Pt–Zn anodes were prepared by depositing zinc onto the cleaned side of the platinum foil, using a standard three-electrode electrochemical cell and a commercially available electroplating solution (Enthobrite CLZ SBR, Enthone GmbH, Langenfeld/Germany) at room temperature. To prevent gas evolution and to maintain the zinc concentration in the plating solution a solid piece of zinc served as counter electrode. With a deposition time of 40 min at 25 mA cm^{-2} the deposition parameters were chosen to yield an approximately 29 µm thick zinc layer (deposition efficiency ~100%, determined by measuring weight before and after deposition).

For thermal alloying the platinum–zinc bi-layers were removed from the polycarbonate frame and clamped between two polished aluminum plates to prevent buckling during alloy formation. Pieces of 25 µm thin aluminum foil (Carl Roth, Karlsruhe/Germany) served as interlayer between the samples and the aluminum holder plates to avert sticking. Annealing was performed in air atmosphere at a temperature of 200 °C for periods of 24, 48, and 96 h. The heating and cooling rate was 170 K per hour in each case. After annealing, extractable zinc was removed by immersing the samples for 2 h in 0.5 M H_2SO_4. Subsequently all samples were re-mounted in the polycarbonate holder and subjected to 10 cyclic voltammetry cycles as described above. Corresponding to their annealing time, the samples are in the following designated as *Pt–Zn_{24}*, *Pt–Zn_{48}*, and *Pt–Zn_{96}*, respectively.

2.2. Nafion modification

In addition, *Pt–Zn_{48}* was also modified by an electro-coated Nafion layer on top of porous Raney-structure, similar to the procedure reported by Rice and Nicholson [23]. Electro-coating is the preferred method to reach uniform Nafion films, involving the electrostatic attraction of negatively charged sulfonate groups in the polymer to the positively charged electrode [20]. Thereto, the electrode was electrically connected with a crocodile clip, which itself was fixed to the extension arm of a dip coater (RDC 15, Bungard Elektronik GmbH, Windeck/Germany). Each sample was then completely immersed in the Nafion solution (5% Nafion 521, Quintech, Göppingen/Germany) and a potential of +1.5 V was applied between the cathode and a platinum wire counter electrode (Ø1 mm, 40 mm long, Chempur, Karlsruhe/Germany). After 120 s the sample was pulled out of the solution at 40 mm min^{-1} while maintaining the potential at +1.5 V. Subsequently, the Nafion layer was cured at 70 °C for 30 min. These samples are designated as *Pt–Zn_{48}*(Nafion). Due to the irregular sample surface the thickness of the Nafion layer could not be determined directly. Therefore a platinum layer sputtered onto silicon was used as substrate in a separate experiment with the deposition process as described above. Here thickness analysis with a surface profiler (Dektak 3030, Veeco Instruments Inc., Plainview/NY) yielded a Nafion layer thickness of approximately (300 ± 20) nm.

2.3. Microstructural evaluation

Roughness factors were estimated from the charge under the hydrogen desorption peaks in the cyclic voltammograms recorded during cleaning of the samples (see Section 2.1), assuming a hydrogen desorption charge of 210 µC cm^{-2} [24] for ideally polished polycrystalline platinum with a roughness factor of 1.

To determine the platinum to zinc ratios of the Raney-platinum anodes a Zeiss DSM 962 scanning electron microscope in combination with an Oxford Instruments INCA300 energy-dispersive X-ray (EDX) system operating at 15 kV was used. Thereto six representative areas (plan view) of approximately 10 μm^2 each were analyzed per sample. The results are presented together with the sample standard variation given in parentheses. Contaminants resulting from preceding sample operation in phosphate buffered saline containing 3.0 mM glucose (including carbon and oxygen) were not considered in the analysis. Samples for imaging of cross-sections by optical microscopy were mounted in epoxy resin and polished carefully to a mirror finish.

The intermetallic phases present in the porosified platinum layers were identified by X-ray powder diffraction, using a PSD (position sensitive detector) transmission diffraction system (Stoe, Darmstadt/Germany) with Cu Kα radiation. From the base platinum foil the porous layer of the samples was scraped off to a powder, and immobilized on a strip of adhesive tape. Eight individual patterns in the range between $2\Theta = 20^\circ$ and 90° were recorded with an exposure time of 800 s, resulting in reflections with high intensity. To suppress artifacts, the eight single patterns were added up to a single pattern.

Lacking reliable data for allowable metal burden, the leaching of zinc was evaluated in terms of metal concentrations resulting from 10-day operation of the electrodes in a given testing volume. To facilitate analysis of the metal traces a volume of 100 ml was chosen, which corresponds to approximately only 7% (approximately 1/15th) of the tissue fluid volume that would be required to sustain the fuel cells oxygen consumption over the 10-day operation period (calculation based on an estimated upper physiological oxygen saturation of 7% ≈0.06 mM [2] and the reduction of oxygen to water in a 4-electron-transfer process [25]). This procedure leads thus to an approximately 15-fold concentration of zinc in the testing solution as compared to actual operation of the fuel cell in a body environment. Taking this into consideration, the significance of zinc leaching from the electrode was evaluated by comparison to physiological normal concentrations in serum. For the experiment a two-chamber fuel cell was constructed from a *Pt–Zn*$_{48}$ anode (2.25 cm^2 in size) and a Raney-platinum cathode fabricated from platinum–aluminum, as described in the second part of this paper series [22]. Anode and cathode were placed in separate polypropylene beakers, each containing 100 ml of phosphate buffered saline (PBS tablets pH = 7.4, containing 0.14 M NaCl, 0.01 M phosphate buffer, and 0.003 M KCl; Invitrogen, Karlsruhe/Germany). The individual beakers were connected via a cotton wick placed in a silicon rubber tube as ion bridge, and the complete assembly was autoclaved at 121 °C for 15 min. After autoclavation, glucose was added to a final concentration of 3.0 mM. Possible deposits formed during autoclavation were then removed by 5 cyclic voltammetry cycles at 10 mV s^{-1} between 1.3 and −0.9 V vs. a saturated calomel reference electrode (SCE), the final cycle ending at −0.5 V to obtain an oxide-free anode. Subsequently the solution was exchanged three times through sterile filters (FP 30/0.2 CA-S, 0.2 μm pore size, Whatman GmbH, Dassel/Germany) against 100 ml of fresh PBS containing 3.0 mM glucose. The anode was then operated for 10 days at a constant current of 40 μA under continuous nitrogen-purging at 37 °C. After this period the concentration of zinc was determined by graphite-furnace atomic absorption spectroscopy (Model 1100B, Perkin Elmer, Waltham/MA), using a single-element hollow cathode lamp. The analysis of the testing solution was repeated 9 times, the result is given as (mean value ± sample standard deviation).

2.4. Electrode assembly

Electrodes were cut into pieces approximately 6 mm × 6 mm in size, and mounted in our previously reported [17] electrode fixtures, exposing a 0.25 cm^2 section of the electrode to the testing solution. To eliminate the influence of contact resistance all samples were equipped with separate platinum wires for electrode current and voltage. The electrode holders were then fixated symmetrically close to the wall of an aseptic electrochemical reactor (as described in [17]), using small amounts of epoxy resin (UHU plus sofort fest, UHU Bühl, Germany). As individual counter electrodes pieces of platinum mesh approximately 1 cm^2 in size were used.

After assembly, the electrochemical reactor was filled with phosphate buffered saline (PBS, see above). To prevent the growth of micro-organisms the complete setup was autoclaved at 121 °C for 15 min. Subsequently glucose was added to the testing solution through a sterile filter (to a final concentration of 3.0 mM). In contrast to our preliminary study [26], the anodes in the present work then underwent 5 cyclic voltammetry cycles at 10 mV s^{-1} between 1.3 and −0.9 V vs. a saturated calomel reference electrode (SCE), as described above. Throughout this procedure the solution was continuously purged with nitrogen at a flowrate of 2 l min^{-1}. Afterwards the testing solution was replaced through the sterile filter with freshly prepared PBS containing 3.0 mM glucose. The complete setup was installed in an incubator to maintain the testing solution at a constant temperature of (37 ± 1) °C.

2.5. Performance characterization

For performance characterization by means of chronopotentiometry the testing environment described elsewhere [17] was employed. In short, the anodes were connected to the individual channels of a computer controlled current sink (STG 2008, Multichannel Systems, Reutlingen, Germany) operating in galvanostatic mode. Electrode potentials were recorded in 5-min intervals against a saturated calomel reference electrode (KE11, Sensortechnik, Meinsberg/Germany).

For the evaluation of different anode fabrication parameters a multi-step chronopotentiometry experiment was performed. Starting from 0 $\mu A\,cm^{-2}$ (open circuit) to a maximum value of 24 $\mu A\,cm^{-2}$, the current density was increased in steps of 8 $\mu A\,cm^{-2}$ every 12 h. Current density–potential plots were then constructed from the anode potentials recorded after 12 h of operation at a given load current. The testing medium throughout these experiments was quiescent de-aerated (headspace nitrogen flow at 2 l min^{-1}, solution initially purged with nitrogen for 1 h) PBS containing 3.0 mM glucose at (37 ± 1) °C. To exclude the influence of electrode history all samples underwent the same experimental sequence. For comparison of polarization behavior, area specific resistances were calculated from the linear slope of the current density–potential curves between 8 and 16 $\mu A\,cm^{-2}$.

Furthermore, after regeneration by cyclic voltammetry (and exchange of the solution as described above), *Pt–Zn*$_{48}$ and *Pt–Zn*$_{48}$(Nafion) anodes underwent a subsequent chronopotentiometry experiment where the current density was kept constant at 8 $\mu A\,cm^{-2}$ for approximately 214 h. The testing solution in this experiment was firstly de-aerated PBS with 3.0 mM glucose. After this experiment the anodes were again regenerated by cyclic voltammetry as described above to exclude the influence of gradual electrode poisoning. Subsequently PBS was exchanged against artificial tissue fluid, and after 6 h at open circuit the chronoamperometry experiment was repeated. The artificial tissue fluid (see Table 1) was prepared from physiological amino acids and taurine, directly dissolved in PBS containing 3.0 mM glucose. Dissolution of the constituents was accelerated by sonication of the solution at 37 °C. The concentrations of the artificial tissue fluid components are listed in Table 1, and were chosen based on the maximum mean concentration in plasma [27,28], or adipose tissue and muscle tissue [29]. To exclude side effects from amino acid degradation

upon prolonged experiments, the chemically unstable glutamine (approximately 30% degradation at pH 8 within 24 h [30]) has been excluded from this mixture. All amino acids were biochemical grade and purchased from VWR (Darmstadt/Germany), except α-amino-n-butyric acid and taurine, which were obtained from Sigma–Aldrich (Munich/Germany). After preparation, the final mixture was stored at −20 °C to prevent decomposition.

For comparison, the *Pt–Zn*$_{48}$ anode was also subjected to chronoamperometry experiments at room temperature (25 ± 2) °C, using a Gamry PCI/350 potentiostat system (Gamry Instruments, Westminster/PA). As base electrolyte quiescent de-aerated 150 mM phosphate buffer (chloride-free, pH = 7.4) containing 100 mM glucose was used, as in the original work on nickel-based Raney-platinum anodes [13] (although the ionic strength was not specified). To show the effect of chloride ions on electrode performance the experiment was also repeated using chloride-containing PBS (see above) as base electrolyte. Before each experiment the anode was regenerated in the respective testing solution by 5 cyclic voltammetry cycles, as described above. After exchange of the solution the anode was held for 6 h at open circuit, during which the potential stabilized. Subsequently the anode was polarized at −290 mV vs. SCE over a period of 24 h.

Throughout the paper roughness factors and potentials are reported as (mean value ± sample standard deviation), whereas bars in graphs represent the minimum and maximum value from triplicate experiments.

Table 1
Composition of the artificial tissue fluid used in the present study.

Component	Concentration μM	Reference	Remarks
α-Amino-n-butyric acid	20	[27,28]	Plasma
Alanine	360	[27,28]	Plasma
Arginine	58	[27,28]	Plasma
Asparagine	56	[27,28]	Plasma
Aspartic acid	62	[29]	Adipose tissue
Citrulline	51	[29]	Muscle tissue
Cystine	49	[27,28]	Plasma
Glutamine acid	66	[29]	Muscle tissue
Glycine	565	[29]	Adipose tissue
Histidine	88	[27,28]	Plasma
Isoleucine	70	[29]	Muscle tissue
Leucine	165	[29]	Muscle tissue
Lysine	186	[27,28]	Plasma
Methionine	21	[27,28]	Plasma
Ornithine	58	[27,28]	Plasma
Phenylalanine	72	[29]	Muscle tissue
Proline	185	[27,28]	Plasma
Serine	195	[29]	Adipose tissue
Taurine	165	[29]	Muscle tissue
Threonine	185	[29]	Muscle tissue
Tryptophane	31	[27,28]	Plasma
Tyrosine	62	[29]	Muscle tissue
Valine	257	[29]	Muscle tissue

3. Results and discussion

3.1. Microstructural evaluation

Fig. 2 shows cross-sections of Pt–Zn samples annealed for 24 and 48 h at 200 °C, both after annealing and subsequent zinc extraction. Not shown is the sample annealed for 96 h at 200 °C, which suffered from severe delamination of the porous layer and was thus not further characterized. When samples were annealed without being clamped between two aluminum plates, the unrestrained platinum–zinc bi-layers buckled and inflected towards the platinum side (data not shown). Delamination can thus be attributed to shear stress, most likely resulting from the considerable mismatch in linear thermal expansion coefficient α between platinum ($\alpha = 8.8 \times 10^{-6}\ K^{-1}$ [31]) and Zn ($\alpha = 30.2 \times 10^{-6}\ K^{-1}$ [31]). In any case, the encountered buckling may be also circumvented by employing e.g. powder metallurgical methods to obtain a homogenous platinum–zinc alloy as starting material for electrode fabrication.

At the interface of the two metals a clearly distinguishable zone of platinum–zinc alloy is formed during heat treatment, which is transformed into a porous layer upon zinc extraction in sulfuric acid (Fig. 2). With the sample annealed for 24 h this results in a crack-free, porous structure of approximately 15 μm thickness, which is well adhering to the bulk platinum foil (Fig. 2a). The longer annealing time of 48 h results in an approximately 30 μm thick porous layer, that in contrast to *Pt–Zn*$_{24}$ exhibits prominent vertical cracks (arrow A in Fig. 2b). These form approximately 2–6 μm wide trenches (arrow B) upon removal of the top zinc layer. Despite the formation of horizontal cracks (arrows C and D in Fig. 2b) in some parts of this sample, the porous layer is still well adhering and mechanically stable.

In Fig. 3 plan view scanning electron micrograph images of the anodes are shown together with the corresponding cyclic voltammograms recorded in de-aerated 0.5 M H_2SO_4. The anodes show a distinctive mud-crack pattern, with primary features in the range of ~1 μm (arrow A in Fig. 3a) for *Pt–Zn*$_{24}$, and up to ~6 μm (arrow B in Fig. 3b) with the longer annealed *Pt–Zn*$_{48}$ samples. At higher magnification nano-porous secondary features in the range of 100–200 nm (arrows C and D in Fig. 3) can be observed for both annealing times.

Regarding the cyclic voltammograms, the Pt–Zn anodes exhibit in principle the electrochemical behavior of platinum (including hydrogen desorption and adsorption, as well as platinum oxidation and its reduction on the backward scan). The compared to literature [24] relatively broad peaks and their poor separation in the hydrogen area are attributed to the highly porous nature of the material. While in the first cycles oxidative current peaks attributable to the dissolution of remaining zinc appear (as shown in Fig. 3), these peaks are not apparent in the subsequent scans, indicating the formation of a chemically stable alloy.

Deduced from the charge under the hydrogen desorption peaks in the cyclic voltammogram, roughness factors of (1889 ± 155) and (2668 ± 179) are obtained upon annealing of the Pt–Zn bi-layers for 24 and 48 h at 200 °C, respectively. For comparison, the blank

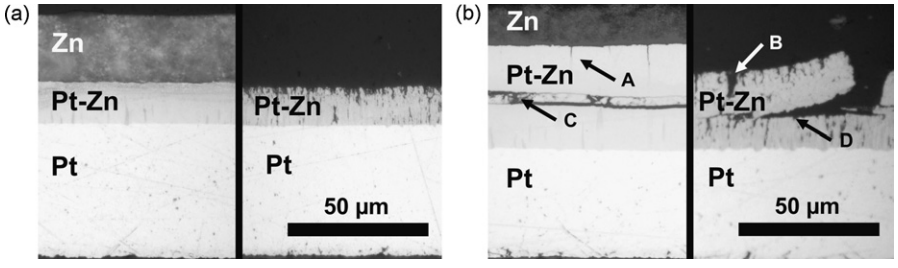

Fig. 2. Cross-sections of Pt–Zn samples annealed for (a) 24 and (b) 48 h at 200 °C, after annealing (left) and subsequent zinc extraction (right). See text for explanations.

platinum foil (unpolished and thus slightly roughened from the foil fabrication process) exhibits a roughness factor of only (31 ± 4).

The increase in roughness factor with annealing time corresponds to the increasing thickness of the nano-porous layer (Fig. 2). Furthermore, the obtained roughness factors are in the range of the values reported by Gebhardt et al. [13] for their Pt–Ni-based Raney film anodes (roughness factors of ~2000, determined by the nitrogen-adsorption BET method).

EDX analysis revealed that a considerable amount of zinc remains in the porosified platinum layer. With platinum to zinc ratios of 3.0:1.0 (±0.2) and 2.5:1.0 (±0.3) there is no significant difference between annealing times of 24 and 48 h, respectively. Also perpendicular to the cross-section (fracture surface), the zinc levels do not differ significantly from the above results (data not shown). With polished cross-sections, as reported in our preliminary study [26], higher levels of zinc have been detected, which resulted from contamination during the polishing process.

To identify the intermetallic phases present in the porosified platinum layer powder diffraction patterns were recorded. Fig. 4(a)–(e) compares the patterns of *Pt–Zn*$_{24}$ and *Pt–Zn*$_{48}$ to the theoretical powder diffraction patterns of crystalline Pt [32], as well as the intermetallic compounds PtZn [33] and Pt_3Zn [34] (data taken from the ICSD-Inorganic Crystal Structure Database [35], FIZ, Karlsruhe/Germany).

As can be seen in Fig. 4, the diffraction patterns do not differ significantly between annealing times of 24 h (*Pt–Zn*$_{24}$) and 48 h (*Pt–Zn*$_{48}$), which corresponds to the EDX results and indicates similar compositions of the porosified layer for both electrodes. Furthermore, the Raney-platinum materials show broad peaks caused by the high porosity of the samples, indicating low ordering of the intermetallic structures. In earlier XRD-investigations of tempered PtZn nanoparticles [36] similar peak broadening caused by lowly ordered material has been observed. Although tempering in general leads to more ordered materials, the longer tempered

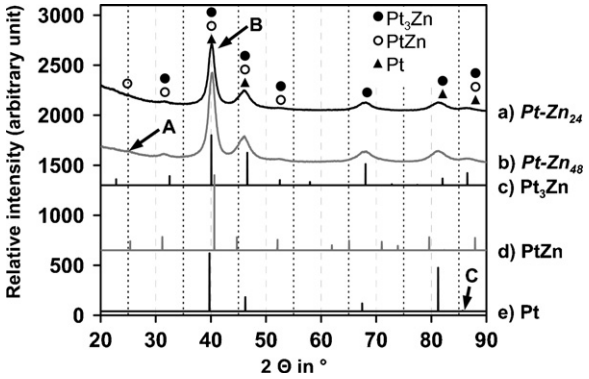

Fig. 4. XRD patterns shown for (a) *Pt–Zn*$_{24}$ and (b) $PtZn_{48}$. Reference data for (c) Pt_3Zn, (d) PtZn and (e) Pt are taken from the ICSD [35]. The correlation of the peaks to the different phases is indicated by circles and triangles; arrow C indicates the position of the small platinum peak not visible at this scale.

Pt–Zn$_{48}$ material does not exhibit significantly sharper peaks. We attribute this to the highly porous nature of the material.

The broad peak maxima render the exact determination of the intermetallic phases difficult, since due to the closely related crystal structures of Pt (Cu-type, $Fm\bar{3}m$, $a = 3.924$ Å), Pt_3Zn (Cu_3Au-type, $Pm\bar{3}m$, $a = 3.893$ Å), and tetragonal PtZn (CuAu-type, $P4/mmm$, $a = b = 2.862$ Å, $c = 3.510$ Å) the majority of the observed peaks overlap, and can thus not exclusively be attributed to a single phase. While several peaks can clearly be assigned to either Pt_3Zn or PtZn (indicated by circles in Fig. 4), the peak onset at around $2\Theta = 25°$ (arrow A in Fig. 4) as well as the positive shift of the peak around $2\Theta = 40°$ (arrow B in Fig. 4) point towards the presence of the PtZn phase. Together with platinum to zinc ratios between 3.0:1.0 (±0.2) and 2.5:1.0 (±0.3) as found by EDX analysis, the XRD results are thus in good agreement with predominant presence of Pt_3Zn as well

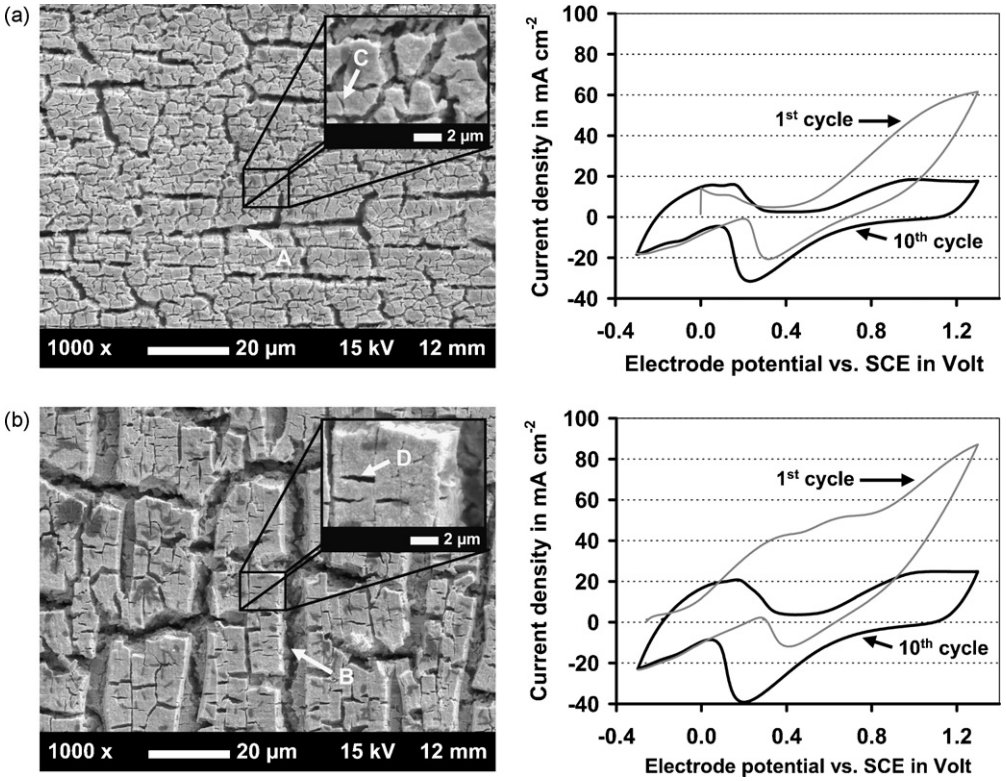

Fig. 3. Plan view micrographs (left) and corresponding cyclic voltammograms (right, 1st and stable 10th cycle) recorded in de-aerated H_2SO_4, shown for (a) *Pt–Zn*$_{24}$ and (b) *Pt–Zn*$_{48}$. See text for explanations.

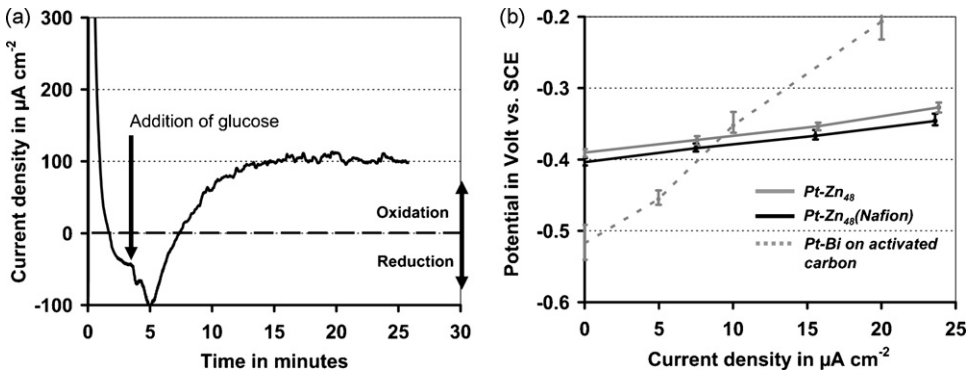

Fig. 5. (a) Chronoamperometry response of a *Pt–Zn*$_{48}$ electrode polarized at −400 mV vs. SCE upon glucose addition to the de-aerated base electrolyte PBS. (b) Current density–potential curves of *Pt–Zn*$_{48}$ and *Pt–Zn*$_{48}$(Nafion) anodes in de-aerated PBS containing 3.0 mM glucose. The performance of the previously reported hydrogel-bound Pt–Bi anode [2] is given for comparison.

as traces of the more platinum-rich PtZn phase in the porosified platinum layer.

In light of the relatively high share of zinc remaining in the electrode, the leaching of trace amounts upon operation of the anode in 3.0 mM glucose in PBS is of particular interest. After 10 days of electrode operation in 100 ml testing solution, a zinc concentration of $(94 \pm 11)\,\mu g\,l^{-1}$ is found. This value is one order of magnitude below the physiological zinc level of $1\,mg\,l^{-1}$ [16] in serum. Even when disregarding the approximately 15-fold concentration of zinc resulting from the employed experimental procedure as compared to actual fuel cell operation in body tissue, the release of zinc can thus be expected to have no significant effect on physiological normal levels.

3.2. Glucose oxidation performance

3.2.1. Analysis of fabrication parameters

In Fig. 5(a) the exemplary response of a *Pt–Zn*$_{48}$ electrode upon glucose addition during a chronoamperometry experiment in de-aerated PBS at room temperature is shown. In the absence of glucose a reductive current is observed, whereas the addition of glucose to a concentration of 3.0 mM leads to the evolution of an oxidative current. This clearly demonstrates the anode's catalytic activity for glucose electro-oxidation and shows that despite the presence of zinc in the electrode (as confirmed by EDX analysis, see above) current generation does not stem from a corrosion process.

The open circuit potentials and area specific resistances from multi-step chronopotentiometry (between 8 and 16 $\mu A\,cm^{-2}$) are summarized in Table 2. While all samples show similar open circuit potentials in the range of −400 mV vs. SCE, *Pt–Zn*$_{24}$ shows a by approximately 1.3 times higher area specific resistance of $(3.11 \pm 0.39)\,k\Omega\,cm^2$, as compared to $(2.35 \pm 0.24)\,k\Omega\,cm^2$ for *Pt–Zn*$_{48}$ and $(2.16 \pm 0.15)\,k\Omega\,cm^2$ for *Pt–Zn*$_{48}$(Nafion). This difference in area specific resistance is in good agreement with the increased true electrode surface of *Pt–Zn*$_{48}$, which is approximately 1.4 times larger compared to *Pt–Zn*$_{24}$.

Fig. 5(b) shows the complete glucose oxidation current density–potential plots of *Pt–Zn*$_{48}$ and *Pt–Zn*$_{48}$(Nafion). As can be seen, the polarization behavior does not differ significantly, although there is a slight tendency of the *Pt–Zn*$_{48}$(Nafion) samples towards more negative electrode potentials. In particular, the presence of the electro-coated Nafion layer has no negative effect on glucose availability at the anode within the investigated current density range, which would be indicated by inflection of the polarization curve towards more positive potentials with increasing current density.

For comparison also the polarization curve of our earlier hydrogel-bound anode is shown, fabricated from activated carbon particles impregnated with platinum–bismuth alloy [2] (recorded with load steps increased in intervals of 24 h in oxygen-free PBS containing 5.0 mM glucose). While these anodes show a by approximately 120 mV more negative open circuit potential, their polarization is more pronounced. Consequently the novel Raney-platinum film anodes presented in this work show up to approximately 100 mV more negative potentials and thus superior performance in the typical fuel cell operating current densities range between 10 and 20 $\mu A\,cm^{-2}$ [2].

To compare the novel zinc-based anodes to Raney-platinum film electrodes fabricated from Pt–Ni alloy foils, chronoamperometry experiments at −290 mV vs. SCE were performed in de-aerated 100 mM glucose solution. While with phosphate buffered saline as base electrolyte the novel anodes exhibit a current density of only 100 $\mu A\,cm^{-2}$ after 24 h, a current density of as much as 386 $\mu A\,cm^{-2}$ is observed upon operation of the *Pt–Zn*$_{48}$ electrode in chloride-free phosphate buffer as used in the original work of Gebhardt et al. [13]. This is close to the current density range reported for Pt–Ni based anodes operated under similar conditions (457–914 $\mu A\,cm^{-2}$; data taken from Fig. 5 in [13]). The lower current density observed in phosphate buffered saline results from chloride ions adsorbed at the anode, which interfere with glucose oxidation [37]. At this point it has to be mentioned that the higher current densities obtained in chloride-free phosphate buffer are of little relevance for practical fuel cell operation in a physiological environment. One the one hand the presence of approximately 140 mM chloride is typical for tissue fluid [38]. On the other hand the practical operating current densities of abiotically catalyzed glucose fuel cells are in the range of only 10–20 $\mu A\,cm^{-2}$ [2,7,13] under physiological conditions, due to the limited availability of oxygen at the cathode [2].

Table 2
Open circuit potentials and area specific resistances of differently fabricated anodes in de-aerated PBS with 3.0 mM glucose (mean value ± sample standard deviation).

Sample designation	Annealing parameters	Open circuit potential mV vs. SCE	Area specific resistance $k\Omega\,cm^2$
Pt–Zn$_{24}$	24 h @ 200 °C	−402 ± 10	3.11 ± 0.39
Pt–Zn$_{48}$	48 h @ 200 °C	−390 ± 5	2.35 ± 0.24
Pt–Zn$_{48}$(Nafion)	48 h @ 200 °C	−404 ± 5	2.16 ± 0.15

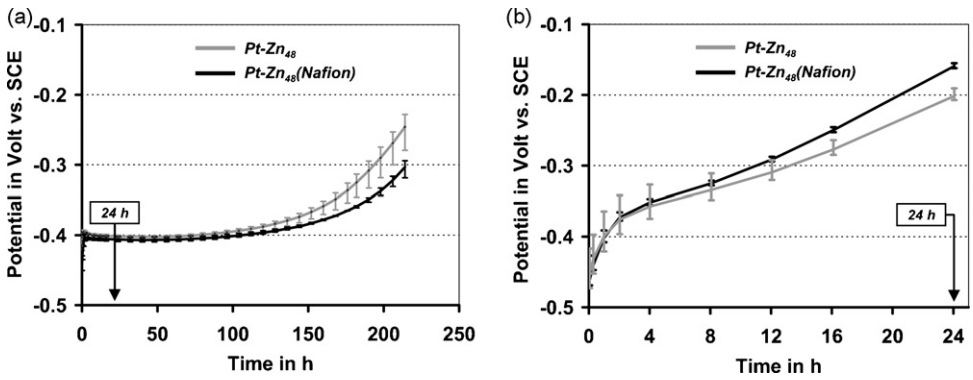

Fig. 6. (a) Glucose oxidation performance of *Pt–Zn*$_{48}$ and *Pt–Zn*$_{48}$(Nafion) at a constant load of 8 μA cm^{-2} in de-aerated PBS with 3.0 mM glucose. (b) Repetition of the experiment in artificial tissue fluid (note the different time scale).

3.3. Long-term performance in PBS and artificial tissue fluid

In Fig. 6(a) the chronopotentiometry results at 8 μA cm^{-2} over a period of 214 h in de-aerated PBS containing 3.0 mM glucose are shown. During the first 100 h of the experiments the electrode potentials of both *Pt–Zn*$_{48}$ and *Pt–Zn*$_{48}$(Nafion) seem to stabilize at a constant potential. However, with increasing operation time a gradually increasing positive shift of anode potential is observed. To rule out the gradual depletion of glucose in the testing solution as cause for this performance degradation, the glucose concentration before the experiment and after 214 h of operation was determined (Accu-Chek test strips, Roche Diagnostics, Mannheim/Germany), yielding no significant decrease in glucose concentration. Furthermore, in separate experiments (data not shown) the observed degradation could not be reversed by exchange of the testing solution against freshly prepared PBS with 3.0 mM glucose. Also in previous investigations such a degradation of platinum-based anodes upon glucose electro-oxidation has been observed, and attributed to electrode poisoning due to adsorbed reaction products, in particular gluconic acid [2,39,40].

The Nafion surface modification of the anode results only in a marginal improvement of long-term stability, which can be attributed to the repulsion of negatively charged gluconic acid by the negatively charged Nafion layer [11,20,41].

The results from repeating the chronoamperometry experiment (after regenerating the anodes by cyclic voltammetry, as described in the experimental section) in artificial tissue fluid are shown in Fig. 6b). When compared to PBS with 3.0 mM glucose, the use of artificial tissue fluid containing amino acids results in a pronounced and rapid positive shift of electrode potential under load. Remarkably, the switch from 3.0 mM glucose in PBS to artificial tissue fluid had no significant effect on the open circuit potential of the anodes (data not shown). This finding corrugates the conclusion of Rao et al. [42] that electrode poisoning by blockage with amino acids or their intermediate products is only partial, so that some active reaction sites for glucose oxidation remain.

In contrast to the results obtained in PBS with 3.0 mM glucose, the Nafion-modified electrodes exhibit even slightly faster degradation in the presence of artificial tissue fluid than the uncoated anode. It can be speculated that this is related to the attraction of positively charged amino acids by the negatively charged Nafion layer. However, for clarification further research beyond the scope of the present work will be required.

4. Conclusion

In the present work we demonstrated that Raney-platinum film anodes with high catalytic activity for glucose oxidation anodes can be fabricated with zinc as alloying partner, replacing the carcinogenic nickel used in previous works. Here the experimental results show that zinc release upon anode operation can be expected to have no significant effect on physiological normal levels, which promises good biocompatibility. This is prerequisite for their intended use in implantable glucose fuel cells. Nevertheless, dedicated cytotoxicity studies will be inevitable to evaluate the interaction of the anode with a body tissue environment.

Besides potential biocompatibility the main advantage of the novel anodes over previous anodes fabricated from hydrogel-bound Pt–Bi catalyst particles is their excellent resistance against oxidative and hydrolytic attack, as demonstrated by acid treatment as integral part of the fabrication process. Furthermore, the novel anodes show significantly lower polarization and thus by up to 100 mV more negative electrode potentials in the current density range relevant for fuel cell operation. However, their long-term stability and tolerance towards artificial tissue fluid demands further optimization, since particularly in artificial tissue fluid a rapid positive shift of electrode potential under load occurs. Possible optimization approaches may include the specific tailoring of the electrode's catalytic properties, e.g. by adatom surface modification with adsorbed bismuth [43,44] to improve poisoning resistance, as well as the application of specifically designed protective polymers with controlled mesh size and charge to repel interfering species [12] such as amino acids. Compared to conventional hydrogel-bound particle anodes, the application of protective polymers will be relatively easy to implement due to the abduction of polymeric hydrogel binders in electrode fabrication. Furthermore, the electrode performance may be improved by increasing the catalytically active surface area. While here the stress-induced delamination encountered with anode fabrication from Pt–Zn bi-layers represents a practical upper limit, a modified fabrication process starting from homogenous Pt–Zn alloys (obtained, e.g. from a fusible regulus [13]) appears as feasible alternative to increase electrode roughness.

The application of the here presented anodes in a complete fuel cell will be reported on in a subsequent publication [45].

Acknowledgements

We gratefully acknowledge financial support from the European Union (contract No. 001837 Healthy Aims), from the Deutsche Forschungsgemeinschaft (DFG) through the PhD program "MicroEnergy Harvesting" (GRK 1322), and from the Ministry for Science, Research, and Arts of the Federal State Baden-Württemberg (co-operation Project "Biopower").

References

[1] S. Kerzenmacher, J. Ducrée, R. Zengerle, F. von Stetten, J. Power Sources 182 (2008) 1–17.
[2] S. Kerzenmacher, J. Ducrée, R. Zengerle, F. von Stetten, J. Power Sources 182 (2008) 66–75.
[3] S.K. Wolfson, S.J. Yao, A. Geisel, H.R. Cash, Trans. Am. Soc. Artif. Int. Organs 16 (1970) 193–198.
[4] P. Malachesky, G. Holleck, F. McGovern, R. Devarakonda, Proceedings of the 7th Intersociety Energy Conversion Engineering Conference, 1972, pp. 727–732.
[5] R.F. Drake, B.K. Kusserow, S. Messinger, S. Matsuda, Trans. Am. Soc. Artif. Int. Organs 16 (1970) 199–205.
[6] G.G. Arzoumanidis, J.J. O'Connell, J. Phys. Chem. 73 (1969) 3508–3510.
[7] J.R. Rao, G. Richter, F. von Sturm, E. Weidlich, Ber. Bunsen Phys. Chem. Chem. Phys. 77 (1973) 787–790.
[8] J.R. Rao, G.J. Richter, F. von Sturm, E. Weidlich, Bioelectrochem. Bioenerg. 3 (1976) 139–150.
[9] Y.M. Maksimov, B.I. Podlovchenko, T.L. Azarchenko, Electrochim. Acta 43 (1998) 1053–1059.
[10] J. Niessen, U. Schroder, M. Rosenbaum, F. Scholz, Electrochem. Commun. 6 (2004) 571–575.
[11] W. Gorski, R.T. Kennedy, J. Electroanal. Chem. 424 (1997) 43–48.
[12] J. Wang, Electroanalysis 3 (1991) 255–259.
[13] U. Gebhardt, J.R. Rao, G.J. Richter, J. Appl. Electrochem. 6 (1976) 127–134.
[14] D.G. Barceloux, J. Toxicol. Clin. Toxicol. 37 (1999) 239–258.
[15] Z. Moser, J. Phase Equilib. Diffusion 12 (1991) 439–443.
[16] S. Caroli, A. Alimonti, E. Coni, F. Petrucci, O. Senofonte, N. Violante, Crit. Rev. Anal. Chem. 24 (1994) 363–398.
[17] S. Kerzenmacher, K. Mutschler, U. Kräling, H. Baumer, J. Ducrée, R. Zengerle, F. von Stetten, J. Appl. Electrochem. 39 (2009) 1477–1485.
[18] R.F.B. Turner, D.J. Harrison, R.V. Rajotte, Biomaterials 12 (1991) 361–368.
[19] D. Moattisirat, V. Poitout, V. Thome, M.N. Gangnerau, Y. Zhang, Y. Hu, G.S. Wilson, F. Lemonnier, J.C. Klein, G. Reach, Diabetologia 37 (1994) 610–616.
[20] M.P. Brazell, R.J. Kasser, K.J. Renner, J. Feng, B. Moghaddam, R.N. Adams, J. Neurosci. Methods 22 (1987) 167–172.
[21] Y.J. Lee, D.J. Park, J.Y. Park, IEEE Sens. J. 8 (2008) 1922–1927.
[22] S. Kerzenmacher, U. Kräling, M. Schroeder, R. Brämer, R. Zengerle, F. von Stetten, J. Power Sources 195 (2010) 6524–6531.
[23] M.E. Rice, C. Nicholson, Anal. Chem. 61 (1989) 1805–1810.
[24] C.H. Hamann, W. Vielstich, Elektrochemie, Wiley-VCH, Weinheim, Germany, 1998.
[25] D. Pletcher, S. Sotiropoulos, J. Electroanal. Chem. 356 (1993) 109–119.
[26] S. Kerzenmacher, J. Ducrée, R. Zengerle, F. von Stetten, Proceedings of Power-MEMS 2007, Freiburg, Germany, 2007, pp. 31–34.
[27] T.L. Perry, S. Diamond, S. Hansen, D. Stedman, Lancet 1 (1969) 806–808.
[28] T.L. Perry, S. Hansen, Clin. Chim. Acta 25 (1969) 53–58.
[29] D.G. Maggs, R. Jacob, F. Rife, R. Lange, P. Leone, M.J. During, W.V. Tamborlane, R.S. Sherwin, J. Clin. Invest. 96 (1995) 370–377.
[30] F.F. Shih, J. Chromatogr. 322 (1985) 248–256.
[31] R.L. Lide, Handbook of Chemistry and Physics, CRC Press, Boca Raton, USA, 2001.
[32] Y. Oya, Y. Mishima, T. Suzuki, Z. Metallkd. 78 (1987) 485–490.
[33] H. Nowotny, E. Bauer, A. Stempfl, Monatsh. Chem. 81 (1950) 1164.
[34] H. Nowotny, E. Bauer, A. Stempfl, H. Bittner, Monatsh. Chem. 83 (1952) 221–236.
[35] A. Belsky, M. Hellenbrandt, V.L. Karen, P. Luksch, Acta Crystallogr. B: Struct. Sci. 58 (2002) 364–369.
[36] A. Miura, H.S. Wang, B.M. Leonard, H.D. Abruna, F.J. DiSalvo, Chem. Mater. 21 (2009) 2661–2667.
[37] E.M. Skou, Acta Chem. Scand. 27 (1973) 2239–2241.
[38] R. Klinke, S. Silbernagel, Lehrbuch der Physiologie, Thieme Verlag, Stuttgart, Germany, 1996.
[39] M.L.B. Rao, R.F. Drake, J. Electrochem. Soc. 116 (1969) 334–337.
[40] H. Lerner, J. Giner, J.S. Soeldner, C.K. Colton, J. Electrochem. Soc. 126 (1979) 237–242.
[41] S.T. Pan, M.A. Arnold, Talanta 43 (1996) 1157–1162.
[42] J.R. Rao, G.J. Richter, G. Luft, F. von Sturm, Biomater. Med. Devices Artif. Organs 6 (1978) 127–149.
[43] S. Kang, J. Lee, J.K. Lee, S.Y. Chung, Y. Tak, J. Phys. Chem. B 110 (2006) 7270–7274.
[44] S. Uhm, H. Jin Lee, Y. Kwon, J. Lee, Angew. Chem. Int. Ed. 47 (2008) 10163–10166.
[45] S. Kerzenmacher, U. Kräling, T. Metz, R. Zengerle, F. von Stetten, J. Power Sources, submitted for publication.